https://doi.org/10.53655/joe.z3238q

Jurnal OptoElektronik

Localized SPR for Pb(II) Ion Sensing Utilizing Chitosan/Reduced Graphene Oxide Nanocomposite

Suraya Abdullah[1], Nur Hidayah Azeman[1, *], Nur Hasiba Kamaruddin[1], Nadhratun Naiim Mobarak[2], and Ahmad Ashrif A Bakar[1, **]

[1]*Department of Electrical, Electronic and Systems Engineering, Faculty of Engineering and Built Environment, Universiti Kebangsaan Malaysia, 43600 Bangi, Selangor, Malaysia*

[2]*Department of Chemical Sciences, Faculty of Science and Technology, Universiti Kebangsaan Malaysia, 43600 Bangi, Selangor, Malaysia*

Corresponding author:nhidayah.az@ukm.edu.my, **ashrif@ukm.edu.my

Keywords

Surface Plasmon Resonance
Chitosan
Graphene Oxide
Nanocomposite
heavy metal

Article History

Received: 29 May 2021
Accepted: 22 June 2021
Published: 15 July 2021

Abstract

In this work, a simple and highly sensitive localized surface plasmon resonance (LSPR) technique had been developed for detection of Pb(II) utilizing chitosan/reduced graphene oxide (CS/rGO) nanocomposite as the sensing material. Gold nanoparticles (AuNP) had been incorporated with the nanocomposite material to induce strong LSPR responses. CS/rGO nanocomposite was coated on top of AuNP and had been utilized as active layer for Pb(II) ion sensing. The morphology and physical properties of gold nanoparticle-chitosan/reduced graphene oxide (AuNP-CS/rGO) nanocomposite was studied using field-emission scanning electron microscopy (FESEM), atomic force microscopy (AFM) and x-ray diffraction (XRD) analysis. FESEM exhibits a rough and wrinkle surface of AuNP-CS/rGO after the addition of rGO. AFM shows a higher surface roughness for AuNP-CS/rGO due to the presence of oxygen atoms in rGO where these oxygen atoms provide more sites for adsorption of Pb(II), hence enhance the sensitivity of the sensor. A good sensitivity of the LSPR sensor for detection of Pb(II) utilizing AuNP-CS/rGO was obtained which is 1.544 ppm^{-1} and the linearity of the sensor are 0.99 and 0.97. In stability study, AuNP-CS/rGO exhibits a good repeatability with relative standard deviation of 2% for 0.01 *ppm*.

1. Introduction

Pb(II) ion detection in environment is crucial due to its hazardous characteristic which harmful to human and environment [1]–[3]. Short and long-term exposure of Pb(II) ion towards human may cause serious health illness such as fatal blood infection [4], behavioural abnormalities, kidney disorders, and neurological impairment [5]. The existing techniques for detection of Pb(II) ion are by costly, bulky and sophisticated instruments such as atomic absorption spectroscopy (AAS) [6], inductively couple plasma mass spectrometry (ICPMS) [7] and inductively couple plasma optical emission spectroscopy (ICP-OES) [8]. Although these techniques provide accurate results, however, they unable to perform in-situ analysis [9]. An ideal Pb(II) ion sensor has to be portable where it has the ability to carry out the analysis on-site with high sensitivity as well as cost-effective.

Recently, localized surface plasmon resonance (LSPR) had been widely utilized for detection of heavy metal ion in environment [1], [10]–[12] due to its advantage of simple, highly sensitive and low-cost. The measurement of LSPR based on wavelength shift is due to the changes in the local dielectric environment caused by the adsorption of analyte [13]. Silver and gold are normally used in LSPR sensing, however due to the biocompatibility and higher chemical stability of gold [14], [15], it is commonly selected over silver in LSPR sensing. The application of materials in LSPR able to improve the gold surface, hence enhance the sensitivity of the LSPR sensors [9]. Various kind of materials had been used for detection of Pb(II) using LSPR such as poly(*m*-phenylenediamine-*co*-aniline-2-sulfonic acid) with detection limit of 0.011 *ppb* [10], monoclonal antibody immobilized onto gold nanoparticle with detection limit of 0.27 *ppb* [16] and glutathione modified $Cu_{2-x}S$ nanocrystals with detection limit of 52.5 *ppb* [17]. Although Pb(II) detection using these materials show low limit of detection, however the preparation of the sensing material is complex and tedious.

Therefore, several groups of researchers had explored the application of chitosan for Pb(II) ion sensing [1], [3], [18]. Chitosan (CS) is a type of polysaccharides which excellent for detecting heavy metal ion due to its water vapour

permeability, mechanical properties and biocompatibility [19], [20]. CS dissolves in weak acetic acid producing a flexible CS film with good mechanical properties which makes it stable and feasible to be applied in the water environment. On top of that, it also possesses good biocompatibility feature, whereas, it is non-toxic and leading to low immunogenicity when exposed to the human body [19], [21], [22]. CS able to adsorb Pb(II) ion due to the presence of amino ($-NH_2$) and hydroxyl (–OH) groups in its structure [11], [19]. The performance of CS can be improved by the incorporation of graphene family with this material. The incorporation of chitosan/reduced graphene oxide nanocomposite able to improve the mechanical strength, electrical conductivity and optical actuation behaviour of the composite for various applications [23], [24]. The large surface area and stability of reduced graphene oxide (rGO) based composite make it suitable for sensing applications [25]. A high sensitivity was obtained for Pb(II) ion detection using gold-chitosan-graphene oxide (Au/CS/GO) nanostructured thin films over gold-chitosan (Au/CS) thin film with sensitivity of 1.11200 ppm^{-1} and 0.77600 ppm^{-1}, respectively [26]. According to Lu *et al.* [27], the hybrids structures of graphene, AuNP and CS provide ultra-sensitive effect towards different Pb(II) ion concentration in the range of 0.5 to 100 $\mu g/L$. In addition, these hybrid films increase the electron transfer between the electrode surfaces due to the hydrophilic channels by CS [28].

In this work, AuNP-CS/rGO nanocomposite was used as a sensing material for detection of Pb(II) utilizing LSPR. The addition of rGO is expected to further improve the mechanical properties of the sensing material as well as providing additional active sites for Pb(II) ion attachment due to the presence of high electronegative atoms on its surface thus leading to the sensor sensitivity enhancement [29]. AuNP was synthesized on the surface of indium tin oxide coated glass slide (ITO/glass) substrate by simple seed mediated technique. CS/rGO was spin-coated on top of AuNP and act as active layer for Pb(II) ion sensing. The stability of AuNP-CS/rGO nanocomposite can be improved through the interaction of positively charged chitosan with the negatively charged rGO [30]. Furthermore, Pb(II) ion can be easily adsorb by chitosan due to the multiple functional groups which chitosan has on its molecular structure such as $-NH_2$ and -OH functional groups [31]. Therefore, the incorporation of AuNP with CS and rGO may enhance the sensitivity of LSPR sensor. The sensitivity of the sensor is determined based on the range of Pb(II) ion concentration used. The structure and morphology of AuNP-CS/rGO are characterized by field emission scanning electron microscopy (FESEM), X-ray diffractometer (XRD) and atomic force microscopy (AFM). The sensor performance such as sensitivity, linearity, and repeatability are discussed accordingly.

2. Experimental Section

2.1 Materials and reagents

Chitosan was obtained commercially from Chito-Chem (Malaysia), Cetyltrimethylammonium bromide (CTAB), glutaraldehyde (GLA), gold chloroauric acid ($HAuCl_4$) and graphene oxide were purchased from Aldrich (USA). L-ascorbic acid and trisodium citrate were purchased from Wako Pure Chemical Industries (Japan), sodium borohydride ($NaBH_4$) was purchased from Merck (Germany). Indium tin oxide (ITO) was commercially obtained from Latech Scientific (Singapore). Acetone, methanol and sodium hydroxide were purchased from R&M Chemicals (Essex, UK). Acetic acid was purchased from Systerm Chemicals (Malaysia). All chemicals were of analytical grade.

2.2 Assembly of AuNP on ITO/glass substrate

ITO coated glass slides (ITO/glass) were cut into 1.0 $cm \times 1.0$ cm size using a diamond glass cutter. Each ITO/glass substrate was cleaned using deionized water, acetone and methanol to ensure that the surface was free from any particulate contamination. The AuNP was grown on the ITO/glass surface by two steps seed-mediated technique at room temperature [32]. Two different solutions were prepared, i.e., the seed solution and the growth solution. The seed solution was prepared by dissolving 0.01 M $HAuCl_4$, 0.5 mL of 0.01 M trisodium citrate and 0.1 mL of 0.1 M ice-cold $NaBH_4$ in 18 mL of deionized water. The seed solution was then placed in an ultrasonic bath for 1 min until a homogenous solution was formed. The resulting dark brown solution indicated that HAuCl4 was successfully reduced by $NaBH_4$. The ITO/glass substrates were immersed in the seed solution, sealed and left undisturbed for 2 hours at room temperature.

The growth solution was prepared by mixing 18 mL of 0.1 M cetyltrimethylammonium bromide (CTAB) with 0.01 M $HAuCl_4$. 0.1 M L ascorbic acid (L-AA) was added into the solution and the solution turned into colourless. Then, 0.1 mL ice-bath sodium hydroxide (NaOH) was added slowly and stirred vigorously until the distinct red colour was observed. The colour of growth solution shows a reflection of the density, shape and size of the nanoparticles [33]. The substrates were immersed in the growth solution for another 2 hours followed by the annealing process.

https://doi.org/10.53655/joe.z3238q

2.3 Preparation of chitosan (CS) solution

Chitosan (CS) solution was prepared by dissolving 0.2 g chitosan with 1 % acetic acid solution. The mixture was vigorously stirred for 2 hours until the solution became homogenous. Then, the CS solution was added with 0.025 mL of glutaraldehyde (GLA) to enhance the stability and hydrophobicity characteristics of crosslinking in CS [1].

2.4 Preparation of reduced graphene oxide (rGO)

Reduced graphene oxide (rGO) was prepared via chemical reduction of graphene oxide [34]. The aqueous graphene oxide (2 mg/mL) was dispersed in 25 mL of deionized water and L-AA. These mixtures were simultaneously stirred at 50 °C and left overnight. The rGO solution was further purified by centrifuged at 3500 rpm and rinsed with deionized water to remove unwanted supernatant. It was then dried in the conventional oven for 2 hours.

2.5 Preparation of chitosan/reduced graphene oxide (CS/rGO) nanocomposite

1 mg of rGO was diluted with deionized water and ultrasonically dispersed for 2 hours. A certain amount of dilute rGO was then mixed with CS solution having a ratio of 1:1.

2.6 Assembly of AuNP-CS/rGO on the ITO/glass substrate

0.1 mL of CS/rGO nanocomposite solution was spin-coated on the surface of the ITO/glass substrate covered by AuNP using a spin-coater (WS-400BX-6NPP/ LITE, Laurell, USA) with the speed of 3000 rpm for 30 seconds and later dried on a hot plate.

2.7 Experimental setup for detection of Pb(II) using LSPR sensor

LSPR measurements technique can be carried out in various ways such as absorptions, transmissions, reflectance, dark-field light-scattering and surface-enhanced raman scattering measurements [13]. The choice of technique is dependent on the types of materials used and research applications. In this work, the measurement of reflectance was applied due to the characteristic of the material used, which is non-transparent in nature. Furthermore, the detection of Pb(II) ion can be carried out in a simplest way by dropping the Pb(II) ion on the prepared AuNP-CS/rGO sensing substrate for analysis.

A simple spectrometer setup consists of a light source (DH-2000-BAL) and a detector (HR4000CG-UV-NIR) from Ocean Optic were used to measure the optical response of nanostructured. A reflection probe with fiber bundle of 6 illumination fibers around 1 read optical fiber was connected to the light source and spectrometer. The fiber core size of each bundle is 600 μm with the reflection probe numerical aperture of 0.22. The probe was adjusted to a minimum distance above the substrate surface as shown in Figure 1. The transmitted light was collected via the read optical fiber in the fiber bundle to the spectrometer.

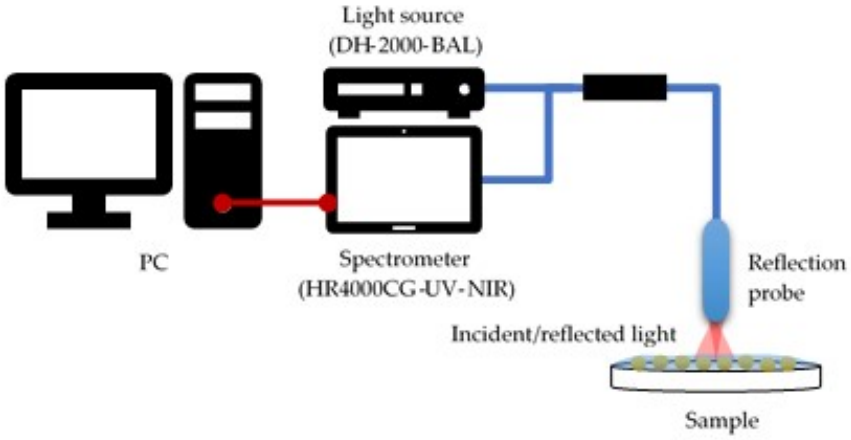

Figure 1. Experimental setup for detection of Pb(II) using LSPR sensor

2.8 Determination of Pb(II) by LSPR

A 1000 ppm of Pb(II) ion stock solution was diluted with deionized water to prepare different concentrations of Pb(II) ion solution in the range of 0.01 – 5.00 ppm. Different concentration of Pb(II) ion solutions were dropped

on the substrate prepared in Section 2.6 and analysed using LSPR measurement. The sensitivity, linearity and repeatability of the sensor was studied.

3. Results

3.1 Characterization of AuNP-CS and AuNP-CS/rGO

In LSPR sensing, AuNP was used to induce strong LSPR responses [35]. Therefore, field emission scanning electron microscopy (FESEM) analysis was carried out to study the surface morphology and interaction between sensing material and substrate. In the first step of seed-mediated technique, when ITO/glass substrate was immersed in the seed solution, Au complex was adsorbed on the surface of ITO/glass substrate. Hereafter, Au(III) in the complex solution was reduced by $NaBH_4$, producing gold nanoparticles (AuNP) dispersed on the ITO/glass substrate surface. After treating the ITO/glass substrate with the growth solution subsequently the first step of seed-mediated technique, the size of the AuNP was increased. The surface morphology of AuNP grown on ITO/glass substrate by seed-mediated technique is shown in Figure 2. As can be seen in the Figure 2, the high density and less aggregated gold nanoparticles on ITO/glass substrate have an average size of 70 *nm*. It was observed that the shape of AuNP was nearly spherical and uniformly distributed on ITO/glass substrate surface.

In the earlier study reported by Zhang and Oyama [36], a seed-mediated growth approach for the attachment and growth of AuNP on ITO/glass substrate surface able to improve the characteristic of AuNP produced, whereby a high density of the dispersed AuNP on the ITO/glass substrate surface was observed, the size and growth of AuNP can be easily controlled and more uniform particle size was produced. Furthermore, the surface of AuNP able to form physical binding to various bio-functional groups via strong bonding interaction of Au-S or Au-N or through physical adsorption [37]. Therefore, to obtain the stability of the colloid, AuNP is coated with an active layer such as polymer that is not sensitive to the slight changes in chemical composition, thus provide sufficient steric hindrance for sensors application [38]. Basically, when AuNP coated with polymer is exposed to heavy metal ion, the dielectric constant around nanoparticle changed, hence change the refractive index due to the interaction of polymer with heavy metal ion, resulting in wavelength shift in the spectrum [38], [39]. The incorporation of AuNP with these capping agents may enhance the sensitivity of the LSPR sensor [37].

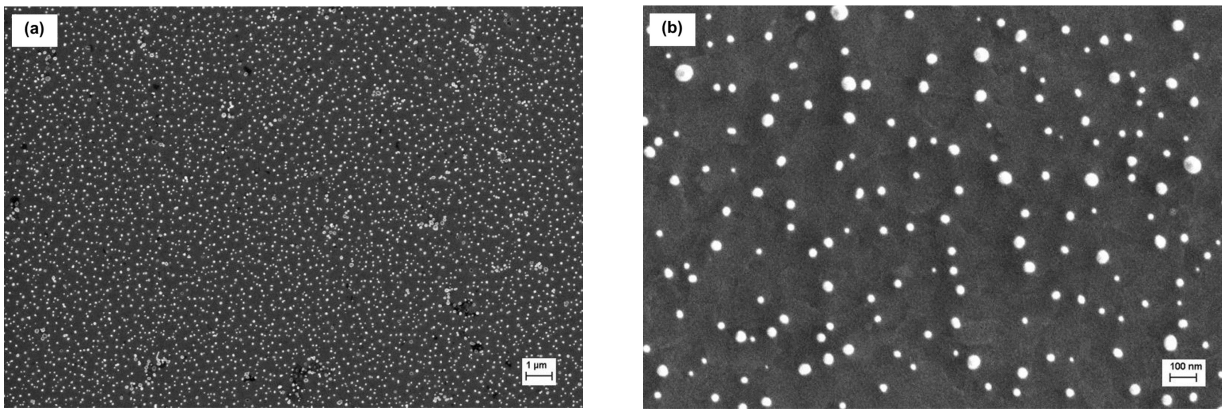

Figure 2. FESEM images of the morphologies of AuNP decorated on the ITO/glass surface using seed-mediated technique at different magnifications.

The AuNP dispersed on ITO/glass substrate surface was coated with CS and CS/rGO which give different surface morphological nature as can be seen in Figure 3. Figure 3(a) shows the surface morphology of AuNP coated with CS layer. It can be observed that AuNP-CS layer was smooth and well dispersed because of hydrophobic characteristic shown by CS [40]. Meanwhile, Figure 3(b) shows the surface morphology of AuNP coated with CS/rGO layer. A rough and wrinkle surface was observed due to the irregular stack of rGO. The addition of rGO into CS able to improve the mechanical properties of CS. This is due to the strong interaction between -OH and -COOH functional groups in rGO with $-NH_2$ group in CS. Therefore, CS can be adsorbed into rGO through hydrogen bonding [41]. It had been reported that rGO provides better dispersion with deionized water compared to graphene, thus less agglomerated structure was observed [42], [43] which makes rGO became homogeneous [44].

Figure 4 shows the three-dimensional (3D) AFM images of (a) AuNP-CS and (b) AuNP-CS/rGO with a scanning size of 10 μm x 10 μm. The surface roughness of the materials can be obtained from the calculation of the root mean square (rms) of roughness [26]. The surface roughness of AuNP-CS and AuNP-CS/rGO were calculated to be 7.542

https://doi.org/10.53655/joe.z3238q

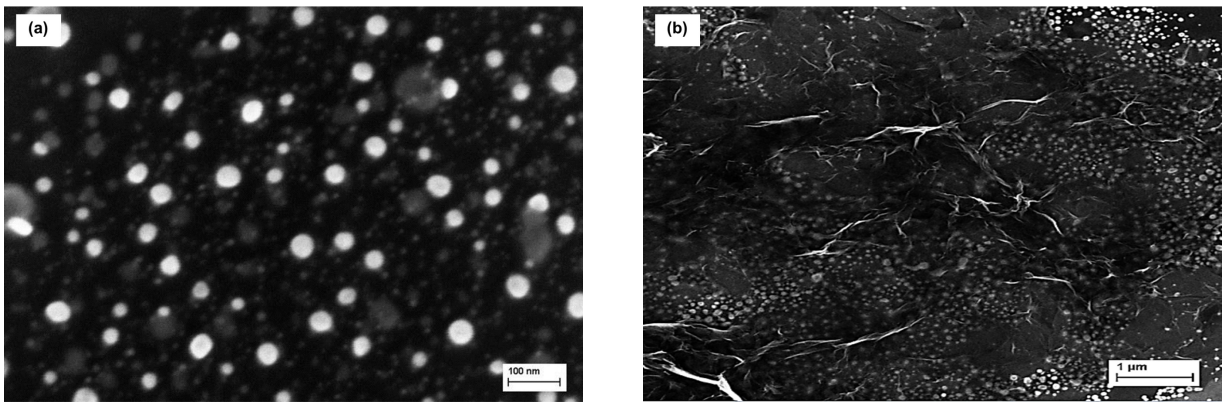

Figure 3. FESEM images of the morphologies of the nanocomposite materials (a) AuNP-CS and (b) AuNP-CS/rGO

nm and 9.484 *nm*, respectively. It was observed that the surface roughness increases when CS/rGO nanocomposite was spin coated on top of AuNP. The higher surface roughness of AuNP-CS/rGO indicated the presence of rGO in the AuNP-CS/rGO nanocomposite due to the presence of oxygen atoms attached to the -OH and -COOH functional groups in rGO [41].

The sensitivity of the sensor system was greatly affected by the surface roughness of the nanocomposite material. High surface roughness of nanocomposite material may increase the mechanical interlocking with polymer chains, thus providing better adhesion at the interface [45]. The presence of high number of oxygen atoms attached to -OH and -COOH functional groups in rGO provides more active sites for adsorption of Pb(II) ion. This phenomenon results in sensitivity enhancement of the sensor system [26]. The grain size of AuNP-CS and AuNP-CS/rGO are 82.9 *nm* and 80.9 *nm* respectively.

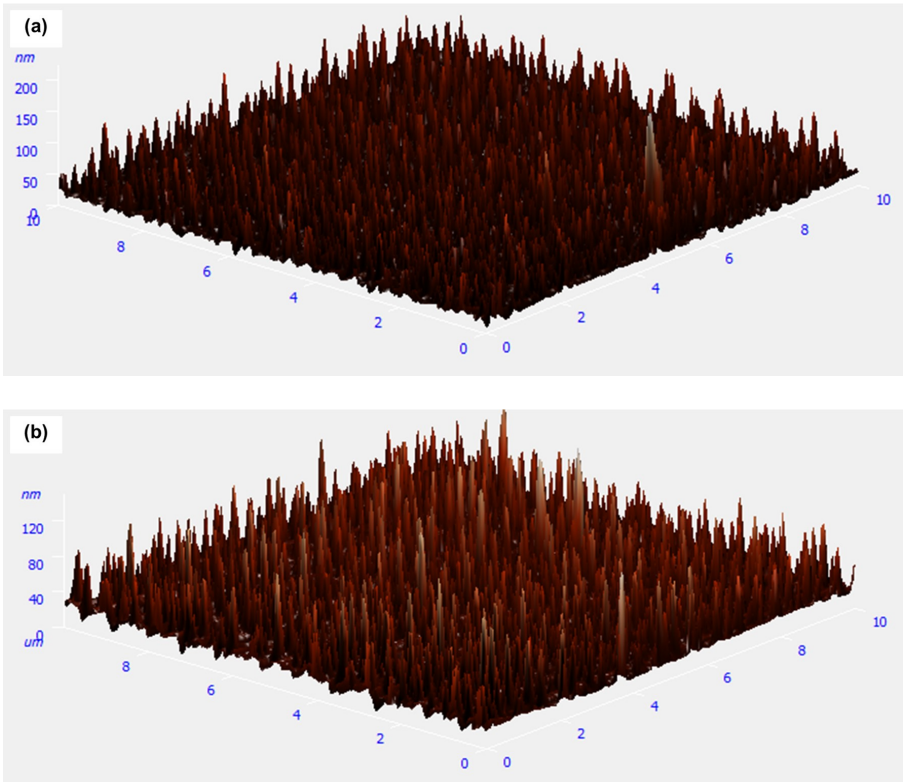

Figure 4. AFM characterization (10 $\mu m \times 10\ \mu m$) (a) AuNP-CS and (b) AuNP-CS/rGO

The XRD analysis was carried out to observe the crystallinity of the structure. Figure 5 shows the XRD patterns of (a) AuNP, (b) AuNP-CS and (c) AuNP-CS/rGO nanocomposite materials. The sharp and intense peaks can be

observed in all three spectrums with two distinct diffraction peaks located at 38.18○ and 44.40○ which corresponds to (111) and (200) planes respectively. The peaks attributed to Au element which indicated a face-centered cubic (fcc) crystalline structure and closely matched with the Joint Committee on Powder Diffraction Standards (JCPDS No. 04-0784) [46]. Meanwhile, in Figure 5(b), two additional peaks with low intensities was observed for AuNP-CS spectrum indicated a reflection from (002) and (220) crystal planes which attributed to CS. This finding shows that the CS could be indexed as orthorhombic crystals (JCPDS No. 39-1894) [47]. Furthermore, as can be seen in the Figure 5(c), an intense peak was observed on the AuNP-CS/rGO spectrum. This data confirmed that AuNP-CS/rGO crystalline is a hexagonal wurtzite structure. The presence of rGO in the nanocomposite structure increases the crystalline of the nanocomposite and the nucleation of crystals in relation to CS [23].

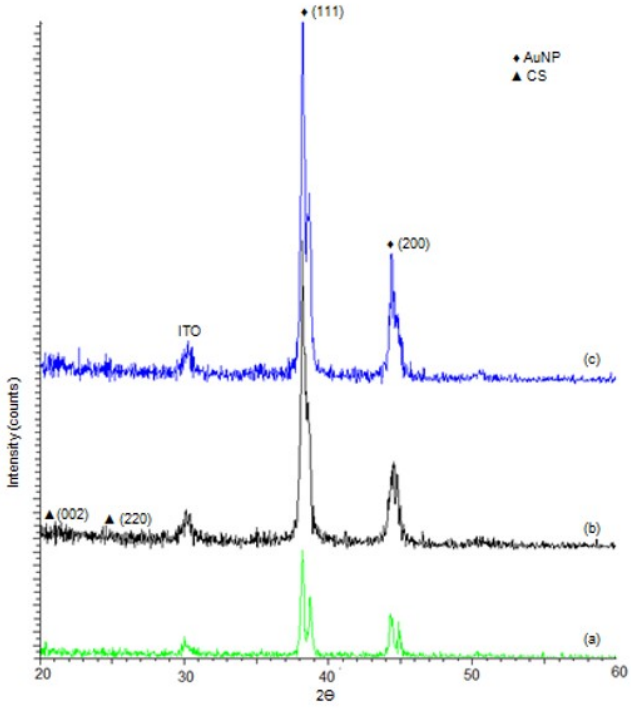

Figure 5. X-ray diffraction patterns of (a) AuNP, (b) AuNP-CS and (c) AuNP-CS/rGO

3.2 LSPR responses of AuNP-CS/rGO nanocomposite material

An LSPR sensor was developed utilizing AuNP-CS/rGO nanocomposite material for the detection of Pb(II) ions. This LSPR sensor could detect as low as part-per-million (ppm) of Pb(II) ion concentration. Figure 6 shows the comparison of the absorption spectra for bare AuNP, AuNP-CS and AuNP-CS/rGO. A broad absorption spectrum at 571 *nm* was observed for AuNP which indicates dipole oscillation with the smooth surface of sphere particles [48]. The polarization was caused by the interaction between AuNP and ITO/glass substrate. The additional of CS layer causes a blue shift in wavelength from 571 *nm* to 568 *nm* due to the decreases in nanoparticle size. The peak of the spectrum became narrower when the positive charge of CS bound to the negative charge of AuNP. This is due to the monodispersity in the size and shape. The addition of rGO exhibits an absorption gap of approximately 3.5 *nm* and the peak become narrower in comparison to AuNP and AuNP-CS. These results indicate that the $\pi - \pi*$ transition in rGO properties enhances the absorption spectra [49].

The performance of LSPR sensor was further studied by applying AuNP-CS/rGO for the measurement of absorptivity for deionized water and different Pb(II) ion concentrations. Deionized water was used as the baseline measurement in this study. The Pb(II) ion solutions were prepared via dilution method at different concentrations of 0.01 *ppm*, 0.5 *ppm*, 1 *ppm*, 3 *ppm* and 5 *ppm*. Figure 7 shows the absorption peak at 572 nm in a visible region when deionized water was dropped onto AuNP-CS/rGO. The wavelength is red-shifted to 576.6, 577.7, 579.5, 580.0 and 581.8 *nm* for 0.01 *ppm*, 0.5 *ppm*, 1 *ppm*, 3 *ppm* and 5 *ppm*, respectively. The shift of the wavelength is due to the increases in refractive index of the nanoparticles whereby the dynamic depolarization was occurred as reported in previous literature [50], [51]. The surface polarization caused the storing in force and the conduction band oscillates

https://doi.org/10.53655/joe.z3238q

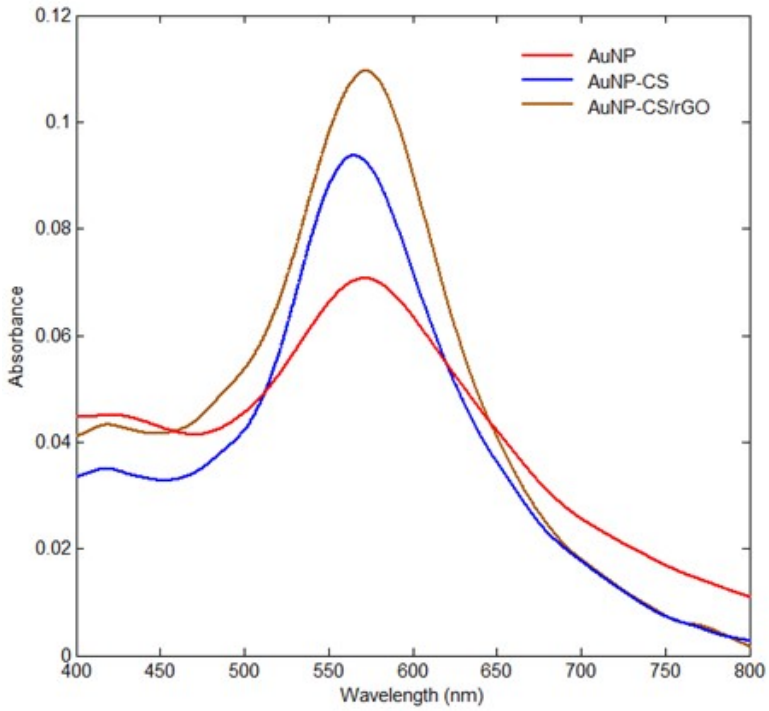

Figure 6. Absorption spectra of AuNP, AuNP-CS and AuNP-CS/rGO

with respect to the positive ion. Furthermore, an increase in Pb(II) ion concentration caused an increase in absorption and changes in refractive index [52].

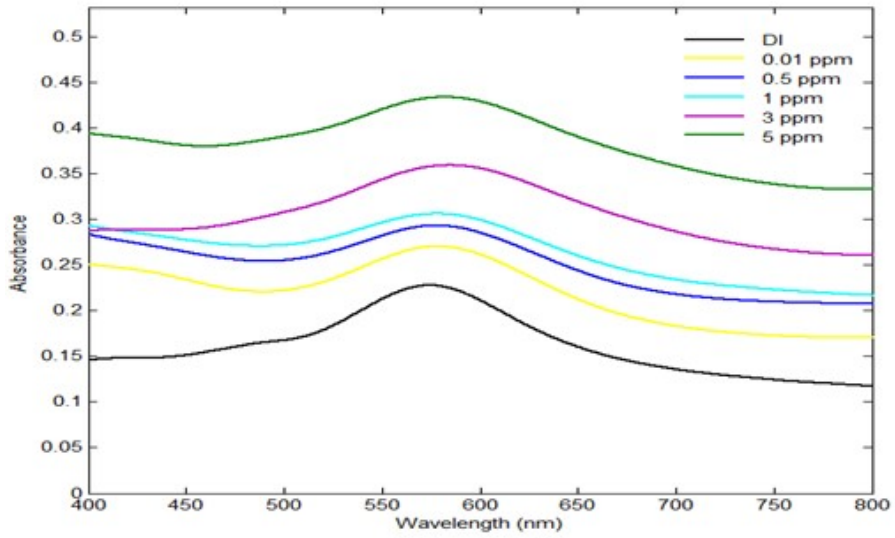

Figure 7. Absorption spectra of deionized water (DI) and different concentrations of Pb(II) ion in the range of $0.01ppm$ to $5ppm$

Figure 8 shows a comparison of the reflectance spectra for bare AuNP, AuNP-CS and AuNP-CS/rGO. As shown in Figure 8, the reflectivity of the peak slightly decreases when CS/rGO was added. A high content of metal caused more light are scattered on the gold nanoparticles surface, thus a higher reflectance peak was observed. The reflectivity decreases to 1.8 % and 5.8 % due to the presence of CS/rGO. This behaviour can be observed by the effect of identical shape and dimension of nanoparticles caused by plasmon resonance between nanoparticles [53]. Interestingly, a smooth surface texture layer of CS and rGO caused a red-shifted in wavelength compared to bare gold nanoparticles.

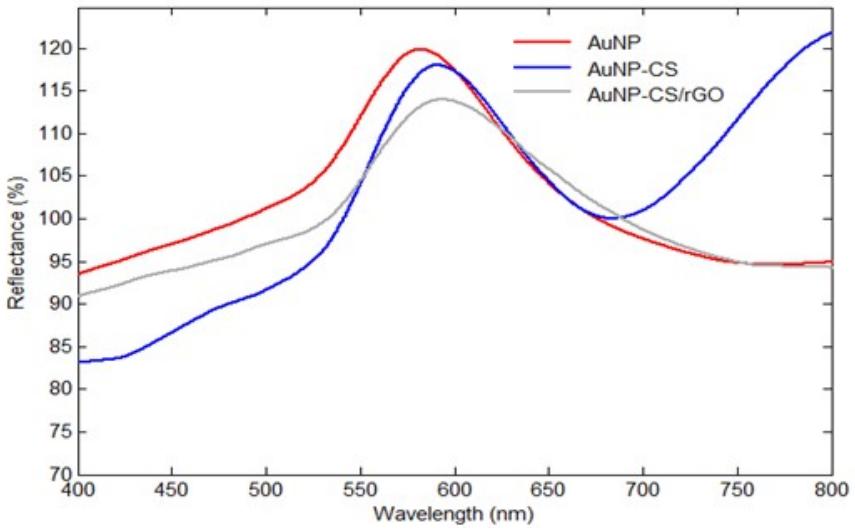

Figure 8. Reflectance spectra of bare AuNP, AuNP-CS and AuNP-CS/rGO

Figure 9 shows the comparison of the reflectance for different concentration range of Pb(II) ion. The intensity of reflectance decreases as concentration increases from 0.01 *ppm* to 5 *ppm*. The reflectance peak of different concentration was measured for 0.01 *ppm*, 0.5 *ppm*, 1 *ppm*, 3 *ppm* and 5 *ppm* at the wavelength of 588.0, 596.3, 596.5, 600.9, 601.7 and 603.2 *nm* respectively. The increased of average refractive index of Pb(II) ion towards AuNP/CS-rGO layer caused a gradual red-shifts in spectrum. The effects of surrounding medium, particles to particles and particles to substrate interaction influence the performance of sensor [51]. Furthermore, the non-detectable properties of ITO/glass substrate widen the peak as stated in the previous literature [54]. It is also worth to mention that the high reflectivity of the sensor is due to the high reflectivity losses of metal nanoparticles on the top flat surface influenced by the backscattering of the nanoparticles itself [55].

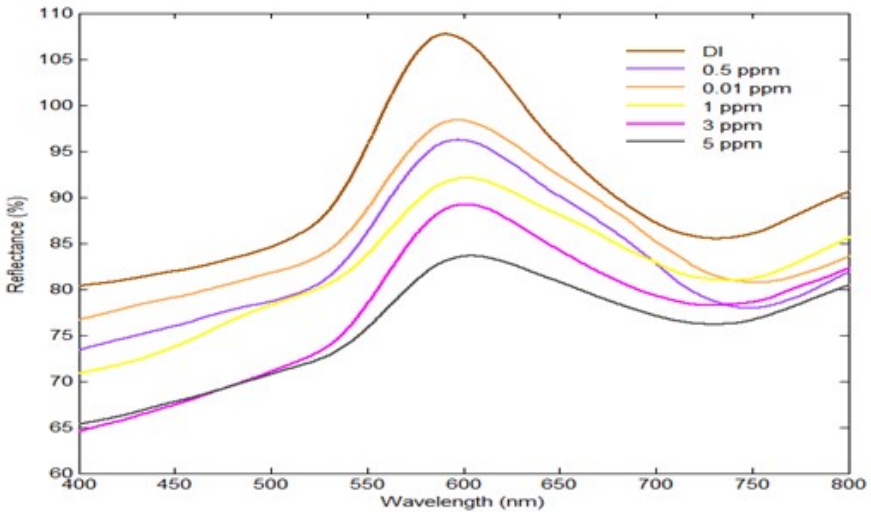

Figure 9. Reflectance spectra of deionized water (DI) and different concentrations of Pb(II) ion in the range of 0.01 *ppm* to 5 *ppm*

Figure 10 shows a good linear regression coefficient of the two regions in the range of 0.01 *ppm* to 5 *ppm* of Pb(II) ion concentration. For 0.01 *ppm* to 1 *ppm*, the linear range was observed as $y = 2.8x + 3.19, (R^2 = 0.99)$ meanwhile for 1 *ppm* to 5 *ppm* is $y = 0.41x + 5.59, (R^2 = 0.97)$. The sensitivity of LSPR sensor was calculated to be 1.544 ppm^{-1} as change in refractive index.

Figure 11 exhibits a calibration curve for the AuNP/CS-rGO LSPR sensor by using the absorbance wavelength peak at 572 *nm*. A good repeatability was obtained for the AuNP/CS-rGO LSPR sensor with relative standard deviation (RSD) of 2 – 4 % for five measurements.

https://doi.org/10.53655/joe.z3238q

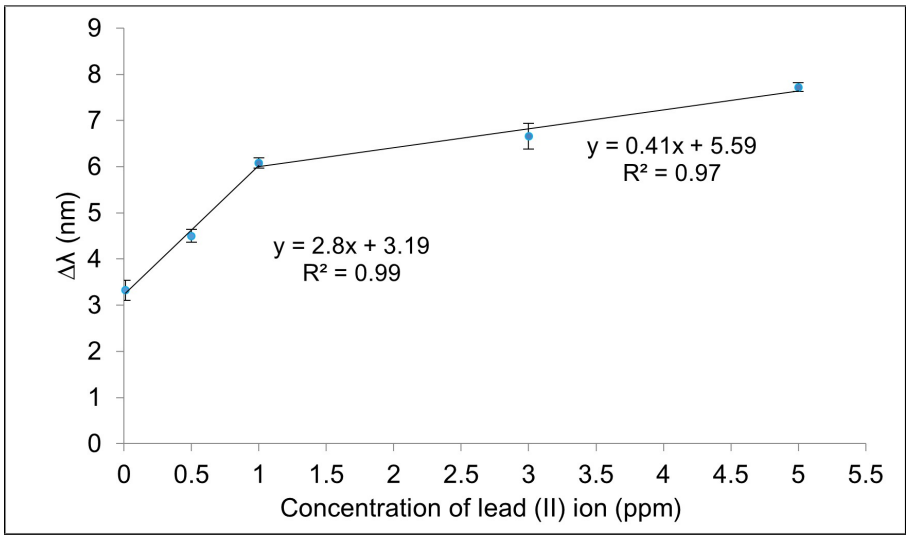

Figure 10. Linear relationship between LSPR wavelength shifts as a function of the concentration of Pb(II) ions

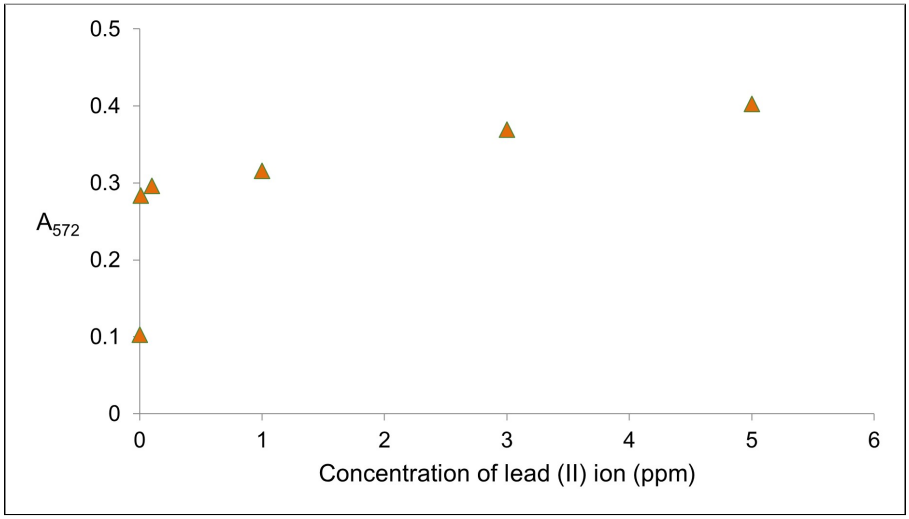

Figure 11. Calibration curves of absorbance value at 572 nm

4. Conclusion

A highly sensitive LSPR sensor of AuNP-CS/rGO for the detection of low concentration in the range of 0.01 *ppm* to 5 *ppm* Pb(II) ion had been successfully developed. The physical morphology of the sensing material affect the performance of the sensor. FESEM shows the presence of rGO caused a rough and wrinkle surface on the sensing material. AFM depicts a higher surface roughness for AuNP-CS/rGO in comparison to AuNP-CS due to the presence of more oxygen atoms attached to the -OH and -COOH functional groups in AuNP-CS/rGO. The LSPR sensor shows a good sensitivity and repeatability when AuNP-CS/rGO surface was exposed to various concentration of Pb(II) due to the presence of -NH2 functional group in CS as well as the presence of –OH and –COOH functional groups in rGO which provide more adsorption sites for Pb(II). The shift in absorption and reflectance spectra demonstrates the fast response in the plasmon peak when CS/rGO layer was exposed to Pb(II) ion. The LSPR sensor performance shows a good linearity of 0.99 and 0.97 with RSD value below 5 % for five measurements.

Conflict of Interest

The authors declare that there is no conflict of interest

Acknowledgments

This research was supported by Photonics Technology Laboratory, Department of Electrical, Electronic and Systems Engineering, Universiti Kebangsaan Malaysia (UKM). The author would also like to acknowledge the financial assistance from Ministry of Higher Education Malaysia (FRGS/1/2018/TK04/UKM/02/6), Universiti Kebangsaan Malaysia (DIP-2019-005).

References

[1] S. Abdullah, N. H. Azeman, N. N. Mobarak, M. S. D. Zan, and A. A. A. Bakar, "Sensitivity enhancement of localized SPR sensor towards pb(II) ion detection using natural bio-polymer based carrageenan," *Optik*, vol. 168, pp. 784–793, Sep. 2018. DOI: 10.1016/j.ijleo.2018.05.016.

[2] N. F. Lokman, N. H. Azeman, F. Suja, N. Arsad, and A. A. A. Bakar, "Sensitivity enhancement of pb(II) ion detection in rivers using SPR-based Ag metallic layer coated with chitosan–graphene oxide nanocomposite," *Sensors*, vol. 19, no. 23, p. 5159, Nov. 2019. DOI: 10.3390/s19235159.

[3] N. H. Kamaruddin, A. A. A. Bakar, M. H. Yaacob, M. A. Mahdi, M. S. D. Zan, and S. Shaari, "Enhancement of chitosan-graphene oxide SPR sensor with a multi-metallic layers of Au–Ag–Au nanostructure for lead(II) ion detection," *Applied Surface Science*, vol. 361, pp. 177–184, Jan. 2016. DOI: 10.1016/j.apsusc.2015.11.099.

[4] J.-H. Park, J.-Y. Byun, S.-Y. Yim, and M.-G. Kim, "A localized surface plasmon resonance (LSPR)-based, simple, receptor-free and regeneratable hg2+ detection system," *Journal of Hazardous Materials*, vol. 307, pp. 137–144, Apr. 2016. DOI: 10.1016/j.jhazmat.2015.12.040.

[5] J. Bi, M. Fang, J. Wang, *et al.*, "Near-infrared fluorescent probe for sensitive detection of pb(II) ions in living cells," *Inorganica Chimica Acta*, vol. 468, pp. 140–145, Nov. 2017. DOI: 10.1016/j.ica.2017.06.044.

[6] H. Ebrahimzadeh and M. Behbahani, "A novel lead imprinted polymer as the selective solid phase for extraction and trace detection of lead ions by flame atomic absorption spectrophotometry: Synthesis, characterization and analytical application," *Arabian Journal of Chemistry*, vol. 10, S2499–S2508, May 2017. DOI: 10.1016/j.arabjc.2013.09.017.

[7] G. Xing, M. R. Sardar, B. Lin, and J.-M. Lin, "Analysis of trace metals in water samples using NOBIAS chelate resins by HPLC and ICP-MS," *Talanta*, vol. 204, pp. 50–56, Nov. 2019. DOI: 10.1016/j.talanta.2019.05.041.

[8] T. Feng, J. Xu, C. Yu, *et al.*, "Graphene oxide wrapped melamine sponge as an efficient and recoverable adsorbent for pb(II) removal from fly ash leachate," *Journal of Hazardous Materials*, vol. 367, pp. 26–34, Apr. 2019. DOI: 10.1016/j.jhazmat.2018.12.053.

[9] A. R. Sadrolhosseini, M. Naseri, and S. A. Rashid, "Polypyrrole-chitosan/nickel-ferrite nanoparticle composite layer for detecting heavy metal ions using surface plasmon resonance technique," *Optics & Laser Technology*, vol. 93, pp. 216–223, Aug. 2017. DOI: 10.1016/j.optlastec.2017.03.008.

[10] G. Qiu, S. P. Ng, X. Liang, N. Ding, X. Chen, and C.-M. L. Wu, "Label-free LSPR detection of trace lead(II) ions in drinking water by synthetic poly(mPD-co-ASA) nanoparticles on gold nanoislands," *Analytical Chemistry*, vol. 89, no. 3, pp. 1985–1993, Jan. 2017. DOI: 10.1021/acs.analchem.6b04536.

[11] B. Feng, R. Zhu, S. Xu, Y. Chen, and J. Di, "A sensitive LSPR sensor based on glutathione-functionalized gold nanoparticles on a substrate for the detection of pb2+ ions," *RSC Advances*, vol. 8, no. 8, pp. 4049–4056, 2018. DOI: 10.1039/c7ra13127e.

[12] G. Qiu, A. H. Law, S. Ng, and C. L. Wu, "Label-free detection of lead(II) ion using differential phase modulated localized surface plasmon resonance sensors," *Procedia Engineering*, vol. 168, pp. 533–536, 2016. DOI: 10.1016/j.proeng.2016.11.516.

[13] K. A. Willets and R. P. V. Duyne, "Localized surface plasmon resonance spectroscopy and sensing," *Annual Review of Physical Chemistry*, vol. 58, no. 1, pp. 267–297, May 2007. DOI: 10.1146/annurev.physchem.58.032806.104607.

[14] L. Singh, R. Singh, B. Zhang, S. Cheng, B. K. Kaushik, and S. Kumar, "LSPR based uric acid sensor using graphene oxide and gold nanoparticles functionalized tapered fiber," *Optical Fiber Technology*, vol. 53, p. 102 043, Dec. 2019. DOI: 10.1016/j.yofte.2019.102043.

[15] M. E. Martinez-Hernandez, J. Goicoechea, and F. J. Arregui, "Hg2+ optical fiber sensor based on LSPR generated by gold nanoparticles embedded in LBL nano-assembled coatings," *Sensors*, vol. 19, no. 22, p. 4906, Nov. 2019. DOI: 10.3390/s19224906.

[16] T.-J. Lin and M.-F. Chung, "Using monoclonal antibody to determine lead ions with a localized surface plasmon resonance fiber-optic biosensor," *Sensors*, vol. 8, no. 1, pp. 582–593, Jan. 2008. DOI: 10.3390/s8010582.

[17] M. Guo, W.-C. Law, X. Liu, *et al.*, "Plasmonic semiconductor nanocrystals as chemical sensors: Pb2+ quantitation via aggregation-induced plasmon resonance shift," *Plasmonics*, vol. 9, no. 4, pp. 893–898, Mar. 2014. DOI: 10.1007/s11468-014-9694-3.

[18] N. Lokman, A. A. Bakar, S. A. Talib, and F. Suja, "SPR response of CS-GO nanostructured thin films for selective detection of pb(II) ions in the saigon river, vietnam," *Desalination and Water Treatment*, vol. 93, pp. 180–186, 2017. DOI: 10.5004/dwt.2017.21407.

[19] N. H. Azeman, N. Arsad, and A. A. A. Bakar, "Polysaccharides as the sensing material for metal ion detection-based optical sensor applications," *Sensors*, vol. 20, no. 14, p. 3924, Jul. 2020. DOI: 10.3390/s20143924.

[20] H. Patel, D. Rawtani, and Y. Agrawal, "A newly emerging trend of chitosan-based sensing platform for the organophosphate pesticide detection using acetylcholinesterase- a review," *Trends in Food Science & Technology*, vol. 85, pp. 78–91, Mar. 2019. DOI: 10.1016/j.tifs.2019.01.007.

[21] K. K. Gadgey and G. S. Sharma, "Investigation of mechanical properties of chitosan based films: A review," *Int. J. Adv. Res. Eng. Technol*, vol. 8, no. 6, pp. 93–102, 2017.

[22] Y. Jiang and J. Wu, "Recent development in chitosan nanocomposites for surface-based biosensor applications," *ELECTROPHORESIS*, vol. 40, no. 16-17, pp. 2084–2097, May 2019. DOI: 10.1002/elps.201900066.

[23] R. Justin and B. Chen, "Strong and conductive chitosan–reduced graphene oxide nanocomposites for transdermal drug delivery," *Journal of Materials Chemistry B*, vol. 2, no. 24, p. 3759, 2014. DOI: 10.1039/c4tb00390j.

[24] M. M.N., S. K.P., and S. A., "Optically triggered actuation in chitosan/reduced graphene oxide nanocomposites," *Carbohydrate Polymers*, vol. 144, pp. 115–121, Jun. 2016. DOI: 10.1016/j.carbpol.2016.02.047.

[25] Y. Zhu, D. Pan, X. Hu, H. Han, M. Lin, and C. Wang, "An electrochemical sensor based on reduced graphene oxide/gold nanoparticles modified electrode for determination of iron in coastal waters," *Sensors and Actuators B: Chemical*, vol. 243, pp. 1–7, May 2017. DOI: 10.1016/j.snb.2016.11.108.

[26] N. F. Lokman, A. A. A. Bakar, F. Suja, *et al.*, "Highly sensitive SPR response of au/chitosan/graphene oxide nanostructured thin films toward pb (II) ions," *Sensors and Actuators B: Chemical*, vol. 195, pp. 459–466, May 2014. DOI: 10.1016/j.snb.2014.01.074.

[27] Z. Lu, S. Yang, Q. Yang, S. Luo, C. Liu, and Y. Tang, "A glassy carbon electrode modified with graphene, gold nanoparticles and chitosan for ultrasensitive determination of lead(II)," *Microchimica Acta*, vol. 180, no. 7-8, pp. 555–562, Feb. 2013. DOI: 10.1007/s00604-013-0959-x.

[28] J. Z. Zhang and C. Noguez, "Plasmonic optical properties and applications of metal nanostructures," *Plasmonics*, vol. 3, no. 4, pp. 127–150, Sep. 2008. DOI: 10.1007/s11468-008-9066-y.

[29] D. T. Nurrohman and N.-F. Chiu, "A review of graphene-based surface plasmon resonance and surface-enhanced raman scattering biosensors: Current status and future prospects," *Nanomaterials*, vol. 11, no. 1, p. 216, Jan. 2021. DOI: 10.3390/nano11010216.

[30] Y. Zuo, J. Xu, F. Jiang, *et al.*, "Voltammetric sensing of pb(II) using a glassy carbon electrode modified with composites consisting of co 3 o 4 nanoparticles, reduced graphene oxide and chitosan," *Journal of Electroanalytical Chemistry*, vol. 801, pp. 146–152, Sep. 2017. DOI: 10.1016/j.jelechem.2017.07.046.

[31] Z. Guo, D.-d. Li, X.-k. Luo, *et al.*, "Simultaneous determination of trace cd(II), pb(II) and cu(II) by differential pulse anodic stripping voltammetry using a reduced graphene oxide-chitosan/poly-l-lysine nanocomposite modified glassy carbon electrode," *Journal of Colloid and Interface Science*, vol. 490, pp. 11–22, Mar. 2017. DOI: 10.1016/j.jcis.2016.11.006.

[32] A. A. Umar, I. Iwantono, A. Abdullah, M. M. Salleh, and M. Oyama, "Gold nanonetwork film on the ITO surface exhibiting one-dimensional optical properties," *Nanoscale Research Letters*, vol. 7, no. 1, May 2012. DOI: 10.1186/1556-276x-7-252.

[33] A. A. Umar and M. Oyama, "Attachment of gold nanoparticles onto indium tin oxide surfaces controlled by adding citrate ions in a seed-mediated growth method," *Applied Surface Science*, vol. 253, no. 5, pp. 2933–2940, Dec. 2006. DOI: 10.1016/j.apsusc.2006.06.038.

[34] J. Zhang, H. Yang, G. Shen, P. Cheng, J. Zhang, and S. Guo, "Reduction of graphene oxide vial-ascorbic acid," *Chem. Commun.*, vol. 46, no. 7, pp. 1112–1114, 2010. DOI: 10.1039/b917705a.

[35] L. Polavarapu, J. Perez-Juste, Q.-H. Xu, and L. M. Liz-Marzan, "Optical sensing of biological, chemical and ionic species through aggregation of plasmonic nanoparticles," *Journal of Materials Chemistry C*, vol. 2, no. 36, p. 7460, Jul. 2014. DOI: 10.1039/c4tc01142b.

[36] J. Zhang and M. Oyama, "Gold nanoparticle arrays directly grown on nanostructured indium tin oxide electrodes: Characterization and electroanalytical application," *Analytica Chimica Acta*, vol. 540, no. 2, pp. 299–306, Jun. 2005. DOI: 10.1016/j.aca.2005.03.054.

[37] Y.-W. Lin, C.-C. Huang, and H.-T. Chang, "Gold nanoparticle probes for the detection of mercury, lead and copper ions," *The Analyst*, vol. 136, no. 5, pp. 863–871, 2011. DOI: 10.1039/c0an00652a.

[38] A. Sugunan, C. Thanachayanont, J. Dutta, and J. Hilborn, "Heavy-metal ion sensors using chitosan-capped gold nanoparticles," *Science and Technology of Advanced Materials*, vol. 6, no. 3-4, pp. 335–340, Jan. 2005. DOI: 10.1016/j.stam.2005.03.007.

[39] Y. Shen, J. Zhou, T. Liu, *et al.*, "Plasmonic gold mushroom arrays with refractive index sensing figures of merit approaching the theoretical limit," *Nature Communications*, vol. 4, no. 1, Aug. 2013. DOI: 10.1038/ncomms3381.

[40] M. Beppu, R. Vieira, C. Aimoli, and C. Santana, "Crosslinking of chitosan membranes using glutaraldehyde: Effect on ion permeability and water absorption," *Journal of Membrane Science*, vol. 301, no. 1-2, pp. 126–130, Sep. 2007. DOI: 10.1016/j.memsci.2007.06.015.

[41] Y. Q. He, N. N. Zhang, W. C. Wang, *et al.*, "Preparation of reduced graphene oxide/chitosan composite films with reinforced mechanical strength," *Advanced Materials Research*, vol. 430-432, pp. 247–250, Jan. 2012. DOI: 10.4028/www.scientific.net/amr.430-432.247.

[42] J. Li, H. Feng, J. Li, *et al.*, "Fabrication of gold nanoparticles-decorated reduced graphene oxide as a high performance electrochemical sensing platform for the detection of toxicant sudan i," *Electrochimica Acta*, vol. 167, pp. 226–236, Jun. 2015. DOI: 10.1016/j.electacta.2015.03.201.

[43] D. Konios, M. M. Stylianakis, E. Stratakis, and E. Kymakis, "Dispersion behaviour of graphene oxide and reduced graphene oxide," *Journal of Colloid and Interface Science*, vol. 430, pp. 108–112, Sep. 2014. DOI: 10.1016/j.jcis.2014.05.033.

[44] Y. Fang, D. Zhang, Y. Guo, Y. Guo, and Q. Chen, "Simple one-pot preparation of chitosan-reduced graphene oxide-au nanoparticles hybrids for glucose sensing," *Sensors and Actuators B: Chemical*, vol. 221, pp. 265–272, Dec. 2015. DOI: 10.1016/j.snb.2015.06.098.

[45] Y. Pan, T. Wu, H. Bao, and L. Li, "Green fabrication of chitosan films reinforced with parallel aligned graphene oxide," *Carbohydrate Polymers*, vol. 83, no. 4, pp. 1908–1915, Feb. 2011. DOI: 10.1016/j.carbpol.2010.10.054.

[46] P. Sharma, G. Darabdhara, T. M. Reddy, *et al.*, "Synthesis, characterization and catalytic application of au NPs-reduced graphene oxide composites material: An eco-friendly approach," *Catalysis Communications*, vol. 40, pp. 139–144, Oct. 2013. DOI: 10.1016/j.catcom.2013.06.021.

[47] J. Gong, X. Hu, K.-w. Wong, *et al.*, "Chitosan nanostructures with controllable morphology produced by a nonaqueous electrochemical approach," *Advanced Materials*, vol. 20, no. 11, pp. 2111–2115, Jun. 2008. DOI: 10.1002/adma.200701840.

[48] J. Rodriguez-Fernandez, A. M. Funston, J. Perez-Juste, R. A. Alvarez-Puebla, L. M. Liz-Marzan, and P. Mulvaney, "The effect of surface roughness on the plasmonic response of individual sub-micron gold spheres," *Physical Chemistry Chemical Physics*, vol. 11, no. 28, p. 5909, 2009. DOI: 10.1039/b905200n.

[49] B. Zahed and H. Hosseini-Monfared, "A comparative study of silver-graphene oxide nanocomposites as a recyclable catalyst for the aerobic oxidation of benzyl alcohol: Support effect," *Applied Surface Science*, vol. 328, pp. 536–547, Feb. 2015. DOI: 10.1016/j.apsusc.2014.12.078.

[50] U. Guler and R. Turan, "Effect of particle properties and light polarization on the plasmonic resonances in metallic nanoparticles," *Optics Express*, vol. 18, no. 16, p. 17 322, Jul. 2010. DOI: 10.1364/oe.18.017322.

[51] K. R. Catchpole and A. Polman, "Plasmonic solar cells," *Optics Express*, vol. 16, no. 26, p. 21 793, Dec. 2008. DOI: 10.1364/oe.16.021793.

[52] J. Cao, E. K. Galbraith, T. Sun, and K. T. Grattan, "Effective surface modification of gold nanorods for localized surface plasmon resonance-based biosensors," *Sensors and Actuators B: Chemical*, vol. 169, pp. 360–367, Jul. 2012. DOI: 10.1016/j.snb.2012.05.019.

[53] C. J. Yi-Tao Long, *Localized Surface Plasmon Resonance Based Nanobiosensors*. Springer-Verlag GmbH, Apr. 2014, 119 pp., ISBN: 9783642547959. [Online]. Available: https://www.ebook.de/de/product/22349031/yi_tao_long_chao_jing_localized_surface_plasmon_resonance_based_nanobiosensors.html.

[54] K. Ariga and M. Aono, "Nanoarchitectonics," *Japanese Journal of Applied Physics*, vol. 55, no. 11, 1102A6, Sep. 2016. DOI: 10.7567/jjap.55.1102a6. [Online]. Available: https://doi.org/10.7567/jjap.55.1102a6.

[55] C. L. Tan, S. J. Jang, and Y. T. Lee, "Localized surface plasmon resonance with broadband ultralow reflectivity from metal nanoparticles on glass and silicon subwavelength structures," *Optics Express*, vol. 20, no. 16, p. 17 448, Jul. 2012. DOI: 10.1364/oe.20.017448.